Numerical simulation of ice accretion on airplane surface

Cite as: AIP Conference Proceedings **2125**, 030013 (2019); https://doi.org/10.1063/1.5117395
Published Online: 26 July 2019

A. A. Aksenov, P. M. Byvaltsev, S. V. Zhluktov, K. E. Sorokin, A. A. Babulin, and V. I. Shevyakov

Numerical Simulation of Ice Accretion on Airplane Surface

A. A. Aksenov[1, a)], P. M. Byvaltsev[2)], S. V. Zhluktov[1)], K. E. Sorokin[3)], A. A. Babulin[4)] and V.I. Shevyakov[4)]

[1]*Joint Institute for High Temperatures RAS, Izhorskaya str. 13, 125412, Moscow, Russia*
[2]*TESIS Ltd., Yunnatov str. 18, 125083, Moscow, Russia*
[3]*Numerical Engineering Platform LLC, Skolkovo innovation center, Nobelja str., 7125373, Moscow, Russia*
[4]*JSC Sukhoi Civil Aircraft, Leninskaya Sloboda str., 26, 115280, Moscow, Russia*

[a)]Corresponding author: andrey@tesis.com.ru

Abstract. Certifying a transport airplane for the flights under icing conditions requires calculations aimed at definition of the dimensions and shapes of the ice formed on the airplane surfaces. Up to date, software developed in Russia for simulation of ice accretion and authorized by Russian certifying supervisory authority, is absent. The paper describes methodology IceVision recently developed in Russia for calculations of ice accretion on airplane surfaces. This methodology is implemented in CFD software FlowVision used by numerous companies and universities in Russia and abroad. The methodology differs from known approaches to simulation of ice accretion. In particular, changing the ice shape is calculated with use of technology VOF. This technology assumes calculations of continuous ice growth accompanied by local rebuilding the computational mesh. The implemented mathematical model provides capability to simulate formation of rime (dry) and glaze (wet) ice. Numerical solutions of validation test problems performed using methodology IceVision are demonstrated.

INTRODUCTION

The procedure of certifying transport airplanes for the flights under icing conditions requires testing aerodynamic models of airplanes in wind tunnels and flight testing of real airplanes with simulators of ice bodies. The shapes and dimensions of the ice bodies are obtained in the flights under natural icing conditions, in the flights behind water-spraying tankers, and in the testing of airplane compartments in special wind tunnels designed for simulation of ice accretion. All these methods are extremely expensive and time-consuming. Therefore, for the time being, different computational methods for definition of the shapes and sizes of the ice accreted on airplane surfaces are actively developed and used all over the world. Commercial software ANSYS FENSAP-ICE and SIEMENS STAR-CCM is widely used for 3D simulation of the ice accretion process. Software developed by the airplane manufacturing companies and by universities, in general, solves only 2D problems.

The first algorithms and methods for calculations of the shapes of ice bodies formed on different solid surfaces have been published at the end of 40-th – beginning of 50-th - see [1, 2]. Those methods were relatively simple. However, the papers defined dry and wet icing regimes and formulated basic ideas of icing simulation. More advanced icing models came out at the end of 70-th – see, for instance, [3]. The paper presents a thermodynamic model for transient growth of ice body on a fixed cylinder due to falling super-cooled water droplets on the surface of the cylinder. The proposed numerical model uses the energy equation, allows simulation of the mixed regime of ice accretion (which permits existence of dry and wet zones), and takes into account different phenomena affecting ice accretion.

By now, different research groups around the world have developed two- and three-dimensional models, methods and algorithms for calculation of the ice body shapes on solid surfaces of airplane in dry and wet regimes. These models, algorithms and methods are implemented in CFD codes: LEWICE (USA) [4 - 6], ONERA (France) [7, 8], TRAJICE (Great Britain) [9, 10], CANICE (Canada) [11, 12], CIRA (Italy) [13], FENSAP-ICE (Canada) [14,

High-Energy Processes in Condensed Matter (HEPCM 2019)
AIP Conf. Proc. 2125, 030013-1–030013-8; https://doi.org/10.1063/1.5117395
Published by AIP Publishing. 978-0-7354-1865-3/$30.00

15], 2DFOIL-ICE (The Netherlands) [16, 17]. Nowadays, the research in numerical simulation of ice accretion is in progress and gives birth to new CFD software, e. g., NSMB-ICE (France) [18, 19], NSCODE-ICE (Canada) [20, 21]. This research is stimulated by increasing strictness of the certifying requirements to airplanes designed for the flights under icing conditions.

Up to date, there is no Russian software designed for numerical simulation of 3D ice accretion, whose results are regarded by certifying supervisory authority as valid ones. The given paper submits an approach to solving 3D problems of ice accretion implemented in Russian CFD software FlowVision [22]. The corresponding mathematical model, the methodology for simulation of ice accretion, and the program module are named *IceVision*. Module IceVision is validated on two test problems: ice accretion on cylinder in dry and wet regimes, ice accretion on airfoil NACA0012 in dry regime. The numerical results are compared against experimental data and calculations in other icing codes.

MATHEMATICAL MODEL

The implemented mathematical model is based on the Euler-Euler (inter-penetrating continua) approach to simulation of multi-phase flows. The gas phase is a mixture of air and water vapor. It is regarded as viscous heat conducting compressible medium. The dispersed phase is composed of super-cooled water droplets. In general case, the velocities and temperatures of the phases are different. The two phases exchange by mass, momentum and energy. Coupled integration of the equations for the continuous and dispersed phases provides the information required for computing the local efficiency of droplets collection, which, in turn, allows one to calculate the distribution of the water flow onto the body surface.

The flow of the carrier phase (wet air) is described by the continuity equation, the momentum equation and the energy equation:

$$\frac{\partial(\phi_c\rho_c)}{\partial t}+\nabla\cdot(\phi_c\rho_c\mathbf{V}_c)=0 \tag{1}$$

$$\frac{\partial(\phi_c\rho_c\mathbf{V}_c)}{\partial t}+\nabla\cdot(\phi_c\rho_c\mathbf{V}_c\otimes\mathbf{V}_c)=-\phi_c\nabla p+\nabla\cdot(\phi_c\hat{\boldsymbol{\tau}}_{eff})-\boldsymbol{Q}_V \tag{2}$$

$$\frac{\partial(\phi_c\rho_c h_c)}{\partial t}+\nabla\cdot(\phi_c\rho_c\mathbf{V}_c h_c)=-\nabla\cdot(\phi_c\boldsymbol{J}_q^{eff})+\frac{d}{dt}(\phi_c p)+\phi_c(\hat{\boldsymbol{\tau}}_{eff}:\hat{\boldsymbol{S}}+\rho\varepsilon)-Q_T \tag{3}$$

Here $\phi_c=1-\phi_d$ is the relative volume of the carrier (gas) phase, ρ_c is the carrier phase density, $\mathbf{V}_c$ is its velocity, p is pressure, $\hat{\boldsymbol{\tau}}_{eff}$ is the effective shear stress tensor, $\boldsymbol{Q}_V$ is the source term due to momentum exchange with the dispersed phase, h_c is the thermodynamic enthalpy of the carrier phase, $\boldsymbol{J}_q^{eff}$ is the effective specific heat flux, $\hat{\boldsymbol{S}}$ the deformation rate tensor, Q_T is the source term due to energy exchange with the dispersed phase.

In addition, the equations for turbulence quantities are solved for the carrier phase. In CFD software FlowVision [22], 7 turbulence models are implemented within URANS approach, in particular, standard k-ε, SA, SST. The calculations discussed below are performed on relatively coarse meshes using wall functions of FlowVision - see [23, 24]. Such calculations are called high-Reynolds calculations. Using wall functions allows one not to resolve the part of the boundary layer adjacent to a solid surface by computational mesh. Instead, pre-defined profiles are used for the sought-for quantities. This approach essentially saves computational resources without loss of accuracy in computing the shear stress and the heat flux at the solid surface.

Within the continual (Euler-Euler) approach, the flow of the dispersed phase (water droplets) is described by the equation for particles transfer, the momentum equation and the energy equation:

$$\frac{\partial n_d}{\partial t}+\nabla\cdot\left(\mathbf{V}_d n_d-\frac{\nu_{t,d}}{Sc_{t,d}}\nabla n_d\right)=0 \tag{4}$$

$$\frac{\partial(n_d\mathbf{V}_d)}{\partial t}+\nabla\cdot\left(\left(\mathbf{V}_d n_d-\frac{\nu_{t,d}}{Sc_{t,d}}\nabla n_d\right)\otimes\mathbf{V}_d\right)=-n_d\frac{1}{\rho_d}\nabla p+\frac{1}{M_d}\boldsymbol{Q}_V \tag{5}$$

$$\frac{\partial\left(n_d T_d\right)}{\partial t}+\nabla\cdot\left(\mathbf{V}_d n_d T_d-\frac{\nu_{t,d}}{Sc_{t,d}}\nabla\left(n_d T_d\right)\right)=\frac{1}{C_{P,d}\left(T_d\right)M_d}\;\;Q_T \tag{6}$$

Here n_d is the particles concentration, ρ_d is the particles (water) density, $\mathbf{V}_d$ is the particles velocity, $\nu_{t,d}$ is the kinematic coefficient of turbulent viscosity assumed equal to that for the gas phase, $Sc_{t,d}$ is the turbulent Schmidt coefficient for the dispersed phase, M_d is the local mass of particles, T_d is the particles temperature, $C_{P,d}$ is the specific heat of particles (of water). The source terms for the interphase exchange by momentum and energy respectively are:

$$\boldsymbol{Q}_V=n_d\rho_c\frac{1}{2}C_D\pi d^2\left|\mathbf{V}_c-\mathbf{V}_d\right|\left(\mathbf{V}_c-\mathbf{V}_d\right) \tag{7}$$

$$Q_T=n_d\pi d^2 Nu_d\frac{\lambda_c}{d}\left(T_c-T_d\right) \tag{8}$$

Here d is the local diameter of particles, λ_c is the heat transfer coefficient of the carrier phase. The following correlations for the particles drag coefficient [25] and for the particles Nusselt number [26] are used in the calculations discussed:

$$C_D=\frac{21.12}{\mathrm{Re}_d}+6.3\,\mathrm{Re}_d^{-0.5}+0.25 \tag{9}$$

$$Nu_d=2+0.55\,\mathrm{Re}_d^{1/2}\,\mathrm{Pr}_c^{1/3} \tag{10}$$

Here $\mathrm{Re}_d=\left(\rho_c\left|\mathbf{V}_c-\mathbf{V}_d\right|d\right)/\mu_c$ is the Reynolds number for particles, μ_c is the dynamic coefficient of viscosity for the carrier phase, $\mathrm{Pr}_c=\left(\mu_c C_{P,c}\right)/\lambda_c$ is the Prandtl number for the carrier phase, $C_{P,c}$ is the specific heat of the carrier phase.

Evaporation of droplets has no effect on the steady-state two-phase flow under the flight conditions discussed. For this reason, the equation for the particles mass is not solved in the current work. Knowledge of the distributions of the particles concentration and velocity near a solid surface allows calculation of the water flow rate onto the surface $\dot{m}_d=\rho_d\mathbf{V}_d^n S$, where S is the area of the solid surface found in a given cell.

The IceVision methodology provides the capability to select dry or wet regime of ice accretion in the FlowVision interface. Rime ice is formed in dry regime, glaze ice is formed in wet regime [27]. In dry regime, the super-cooled water droplets completely freeze immediately after impingement onto a solid surface. In wet regime, only part of water freezes. Another part forms a water film which flows over the airplane or ice surface under the action of aerodynamic forces. The implemented mathematical model automatically identifies zones of rime and glaze ice in wet regime. It should be mentioned that the wet regime is the most interesting from the practical point of view and the most complex from the point of view of numerical simulation.

The methodology proposed in the given paper essentially differs from the approaches implemented in other icing codes (ANSYS FENSAP_ICE, LEWICE etc.): 1) In module IceVision, evolution of the ice shape is calculated using technology VOF. The general algorithm implies simultaneous calculations of the external two-phase flow, ice heating and motion of the contact surface. Therefore, this technology provides continuous ice growth. Notice that although the time step, characterizing ice growth, may exceed the time step, characterizing the external flow, by two orders of magnitude, it remains small with respect to the entire icing time. 2) Displacement of the contact surface initiates local regeneration of the computational mesh. However, the mesh is rebuilt only in the cells containing the ice surface. All the other cells remain the same.

The energy balance at the ice surface allows for conjugate heat exchange between air and ice, latent heat of crystallization and latent heat of evaporation / sublimation:

$$\left(h_d-h_f\right)\;\dot{m}_d\;+\left(\lambda_c+\lambda_{c,t}\right)\frac{T_{cell,c}-T_{wall}}{y_{cell,c}}-\;\dot{m}_{evap(subl)}\,\Delta h_{evap(subl)}=\lambda_i\frac{T_{wall}-T_{cell,i}}{y_{cell,i}}-\;\dot{m}_i\;\;\Delta h_{fusion} \tag{11}$$

Here index «*cell*» stands for the value in the center of a cell adjacent to ice, $\dot{m}_{evap(subl)}$ is the vapor flow rate due to evaporation of water or sublimation of ice, $\dot{m}_i$ is the icing rate of water coming with droplets onto the ice surface, $\lambda_{c,t}$ and λ_i are the turbulent heat conductivity of gas and the heat conductivity of ice, h_d and h_f are the thermodynamic enthalpy of water and that of ice, $\Delta h_{evap(subl)}$ and Δh_{fusion} are the latent heats of evaporation / sublimation and fusion (positive quantities), $T_{cell,c}$ and $T_{cell,i}$ are the temperatures of gas and ice in the centers of the neighbor cells adjacent to the contact surface, T_{wall} is the temperature of the contact surfaces which is assumed equal to the film temperature $T_{wall} = T_0 = 273{,}15(^\circ C)$ in the wet regime, $y_{cell,c}$ and $y_{cell,i}$ are the distances from the centers of the adjacent cells to the contact surface. The thermodynamic enthalpy of a substance is determined by

$$h_{subst}(T) = h_{subst,0}(298.15) + \int_{298.15}^{T} C_{p,subst}(T)\,dT \tag{12}$$

The vapor mass flow rate from the film or air-ice contact surface specific is found from the following algebraic equation:

$$\dot{m}_{evap(subl)} \cdot (1 - Y_{wall,vap}) = \left(\frac{\mu_c}{Sc_c} + \frac{\mu_{c,t}}{Sc_{c,t}} \right) \frac{Y_{wall,vap} - Y_{cell,vap}}{y_{cell,c}} \tag{13}$$

Here $\mu_{c,t}$, $Sc_c, Sc_{c,t}$ respectively are the dynamic coefficient of turbulent viscosity, the molecular and turbulent Schmidt numbers for the carrier phase. Integration of the mass transfer equation for the carrier phase yields the mass fraction of vapor in the center of a cell adjacent to ice $Y_{cell,vap}$. The mass fraction of vapor at the contact surface is computed from

$$Y_{wall,vap} = X_{wall,vap} \frac{m_{vap}}{m_{wall,c}} \tag{14}$$

where $m_{wall} = X_{wall,vap} m_{vap} + (1 - X_{wall,vap}) m_c$ is the local molar mass of the carrier phase (an air- vapor mixture) at the contact surface, m_{vap}, m_c respectively are the molar masses of vapor and air. The molar fraction of vapor at the contact surface is determined by

$$X_{vap,w} = \frac{p_{vap,sat}(T_{wall})}{p} \tag{15}$$

where $p_{vap,sat}(T)$ is the tabulated dependency of the saturated vapor pressure on temperature.

Icing rate $\dot{m}_i$ is computed from Eq. (11). This quantity serves as a source term in the mass conservation equation for the ice phase. Solving this equation yields the relative volume of ice in each computational cell (variable VOF). The contact surface is reconstructed using the distribution of variable VOF at the each time step. In the ice phase, the energy equation is solved with respect to the thermodynamic enthalpy of ice h_i:

$$\rho_i \frac{\partial h_i}{\partial t} = \nabla \left(\frac{\lambda_i}{C_{P,i}} \nabla h_i \right) \tag{16}$$

where ρ_i and $C_{P,i}$ respectively are the density and specific heat of ice.

In wet regime, the water mass flow rate into the film is computed from

$$\dot{m}_f = \dot{m}_d - \dot{m}_i - \dot{m}_{evap(subl)} \tag{17}$$

The equation for the film transfer is derived from the mass conservation law. It is solved with respect to the relative volume of film f. The equation can be written in discrete form as follows:

$$\frac{f_{cell}^{n+1} - f_{cell}^{n}}{\Delta \tau_f} + \sum_{sides} F_{side} = \frac{S_{cell,base}}{\Omega_{cell} \rho_d} \dot{m}_f \tag{18}$$

Here Ω_{cell}, $S_{cell,base}$ respectively are the volume of a cell adjacent to ice and the ice area in the cell, $\Delta\tau_f$ is the explicit time step used for integration of the film transfer equation. The film flow into a neighbor cell containing the ice surface is computed using upwind scheme as follows:

$$F_{side} = \begin{cases} \left(\left|\mathbf{V}_{cell,f}\right| \cdot h_{cell,f} \cdot L_{side}\right) / \Omega_{cell}, & \mathbf{V}_{cell,f} \cdot \boldsymbol{n} > 0 \\ \left(\left|\mathbf{V}_{nei,f}\right| \cdot h_{nei,f} \cdot L_{side}\right) / \Omega_{cell}, & \mathbf{V}_{nei,f} \cdot \boldsymbol{n} < 0 \end{cases} \tag{19}$$

Here index «*nei*» stands for the value of a quantity in a neighbor cell adjacent to ice. Vector $\boldsymbol{n}$ is the normal to the face separating two cells adjacent to the ice surface. It points from the current cell to the neighbor one. A linear profile of the water velocity in the film is assumed. Consequently, the mean film velocity linearly depends on the film thickness $h_{cell,f}$:

$$\mathbf{V}_{cell,f} = \frac{h_{cell,f}}{2\mu_d} \boldsymbol{\tau}_{cell,w} \tag{20}$$

Here $\boldsymbol{\tau}_{cell,w}$ is the shear stress vector or viscous force exerted onto the ice surface by the gas phase. The film thickness is determined by

$$h_{cell,f} = \frac{f \cdot \Omega_{cell}}{S_{cell,base}} \tag{21}$$

It is assumed that the film separates from a solid surface when condition (19) cannot be satisfied because the film velocities in the neighbor cells have opposite directions with respect to the inter-cell face.

VALIDATION

The mathematical model and methodology implemented in program module IceVision are validated on two test problems: ice accretion on cylinder in dry and wet regimes, ice accretion on airfoil NACA0012 in dry regime.

Ice accretion on cylinder was selected as basic validation test problem. The cylinder diameter is $0.025\ (m)$. The free stream of air contains super-cooled water droplets. The free stream conditions are: pressure $p_\infty = 101000\ (Pa)$, velocity $V_\infty = 70\ (m/s)$, mean droplet diameter $MVD = 20\ (\mu m)$, liquid water content $LWC = 0.5\ (g/m^3)$. Dry regime assumes free stream temperature $T_\infty = 253.15\ (K)$. Wet regime assumes free stream temperature $T_\infty = 265.15\ (K)$. The collection efficiency and ice shapes calculated in FlowVision+IceVision are compared against the results obtained in software Fluent FENSAP-ICE – see Figs. 1 and 2. One can see good qualitative and quantitative agreement between the IceVision and FENSAP-ICE results.

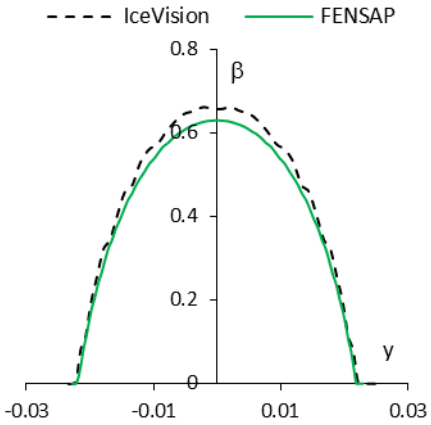

FIGURE 1. Distribution of local collection efficiency β over the cylinder surface

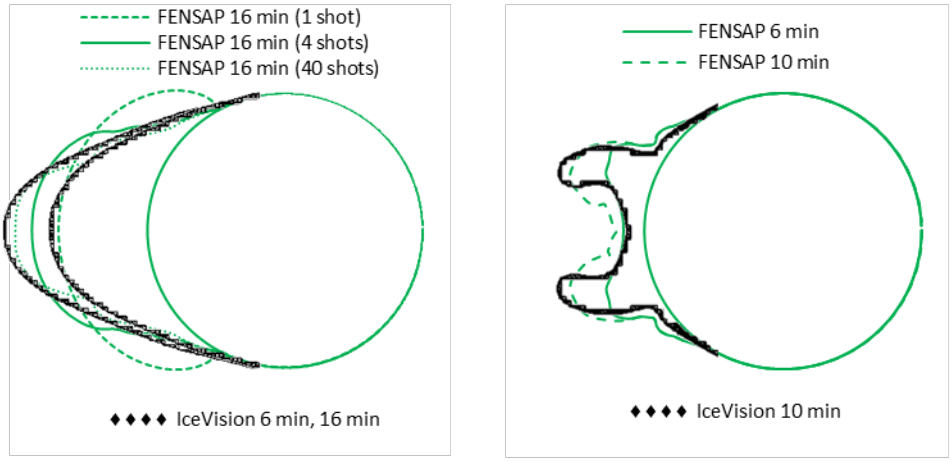

(a) (b)

FIGURE 2. Ice shapes on cylinder at different time points counted from the start of icing in dry regime (a) and wet regime (b)

In addition, ice accretion on airfoil NACA0012 was simulated. For validation purposes, two different cases are considered. The free stream conditions for these cases are: 1) pressure $p_\infty = 101000\,(Pa)$, velocity $V_\infty = 102.8\,(m/s)$, mean droplet diameter $MVD = 20\ (\mu m)$, liquid water content $LWC = 0.5\,(g/m^3)$, temperature $T_\infty = 256.49\,(K)$ and 2) $p_\infty = 101000\,(Pa)$, $V_\infty = 67.1\,(m/s)$, $MVD = 20\ (\mu m)$, $LWC = 1\,(g/m^3)$, $T_\infty = 244.51\,(K)$. These conditions correspond to dry regime of ice accretion. For this reason, "Dry icing" option has been selected in the FlowVision interface. The experiment on the ice accretion on airfoil NACA0012 under the same conditions (IRT RUN 404 and RUN 425) has been carried out in climatic wind tunnel NASA Glenn Icing Research Tunnel (IRT) [5]. The experimental results have been used as benchmark data for validation of the most of known icing codes including commercial software LEWICE and FENSAP-ICE. The dimensions of the computational domain created in FlowVision are 45 x 45 chords. Initial grid was condensed around the foil using the built-in grid generator. Besides that, local adaptation to the foil surface was specified in the FlowVision interface. The resulting grid was generated automatically. The size of the cells adjacent to the foil surface is characterized by value Y+ ≈ 50. Figure 3 demonstrates the steady-state distribution of the Mach number around the airfoil without icing (module IceVision being inactive).

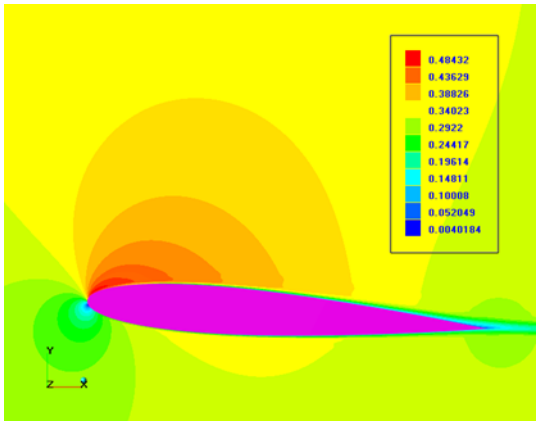

FIGURE 3. Steady-state distribution of the Mach number around airfoil NACA0012 without icing

Figure 4 relates to IRT RUN 404 and compares the calculations of collection efficiency β performed in software FlowVision+IceVision with published numerical results obtained in software LEWICE [4-6].

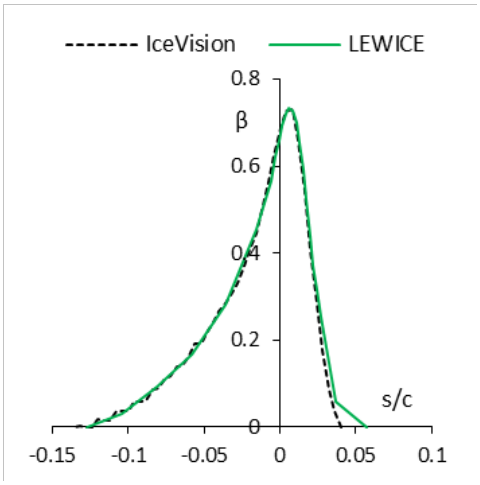

FIGURE 4. Distribution of local collection efficiency β over the surface of airfoil NACA0012

Figure 5 shows the ice shape computed using technology IceVision and the shape obtained in the experiment (IRT RUN 425). One can see that even irregularities in the two shapes coincide quite well.

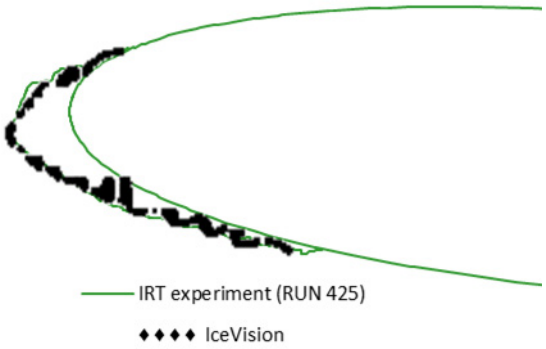

FIGURE 5. Computed (dotted line) and experimental (solid line) shapes of ice on airfoil NACA0012 after 6 minutes from the start of icing

CONCLUSION

This paper presents the mathematical model and methodology for calculation of the ice accretion process. The model is implemented in program module IceVision. The module enters CFD software FlowVision. The model automatically identifies zones of rime and glaze ice. In a rime (dry) ice zone, the temperature of the contact surface between air and ice is calculated with account of ice sublimation and heat conduction in ice. In a glaze (wet) ice zone, the water film flow is taken into account. The submitted mathematical model is completely based on the Euler multi-speed approach to simulation of multi-phase flows. The computational algorithm allows for essentially different time scales for physical processes proceeding in the course of ice accretion, viz., air flow, water flow, and ice growth. Validation of the model is demonstrated. Analysis of the obtained results shows that the numerical solutions obtained in module IceVision agree well with experimental data and calculations in other icing codes.

REFERENCES

1. F. H. Ludlam, Quarterly Journal of the Royal Meteorological Society **77**(1), 663–666 (1951).
2. B. L. Messinger, Journal of the Aeronautical Sciences **20**(1), 29–42 (1953).
3. F. H. Lozowski, J. R. Stallabras and P. F. Hearty, "The icing of an unheated non-rotating cylinder in liquid water droplet-ice crystal clouds", National Research Council (NRC). Laboratory report LTR-LT-96, 1979.
4. W. B. Wright, "User's manual for the Improved NASA Lewis ice accretion code LEWICE 1.6", National Aeronautical and Space Administration (NASA), Contractor Report, 1995.
5. W. B. Wright and A. Rutkowski, "Validation results for LEWICE 2.0", NASA, Tech. rep. CR 1999–208690, 1999.
6. W. Wright, P. Struk, T. Bartkus and G. Addy, "Recent advances in the LEWICE icing model", in SAE Technical Paper 2015-01-2094, 2015.
7. D. Guffond and R. Hedde, "Henry Overview of icing research at ONERA, Advisory Group for Aerospace Research and Development", in *Fluid Dynamics Panel (AGARD/FDP) Joint International Conference on Aircraft Flight Safety – Actual Problems of Aircraft Development* (Zhukovsky, Russia, 1993), 7 p.
8. E. Montreuil, A. Chazottes, D. Guffond, A. Murrone, F. Caminade and S. Catris, "Enhancement of prediction capability in icing accretion and related performance penalties; part i: Three-dimensional cfd prediction of the ice accretion", in *1st AIAA Atmospheric and Space Environments Conference* (San Antonio, TX, 2002) AIAA Paper 2009-3969.
9. R. W. Gent, "TRAJICE2, a combined water droplet and ice accretion prediction program for aerofoil", Royal Aerospace Establishment (RAE). — Farnborough, Hampshire, Tech. rep. No. TR90054, 1990.
10. W. B. Wright, R. Gent and D. Guffond, "DRA/NASA/ONERA collaboration on icing research part II - prediction of airfoil ice accretion", NASA, Tech. rep. CR–202349, 1997.
11. P. Tran, M. T. Brahimi, I. P. A. Paraschivoiu and F. Tezok, "Ice accretion on aircraft wings with thermodynamic effects" in *American Institute of Aeronautics and Astronautics, 32-nd Aerospace Sciences Meeting and Exhibition* (Reno, NV, 1994) AIAA paper No. 0605, 9 p.
12. A. Pueyo, D. Chocron and F. Kafyeke, "Improvements to the ice accretion code CANICE", in *Proceedings of the 8th Canadian Aeronautics and Space Institute (CASI) Aerodynamic Symposium* (Toronto, Canada, 2001) 9 p.
13. G. Mingione and V. Brandi, Journal of Aircraft **35**(2), 240—246 (1998).
14. H. Beaugendre, F. Morency and W. G. Habashi "ICE 3D, FENSAP-ICE'S 3D In-Flight Ice Accretion Module", in *American Institute of Aeronautics and Astronautics, 40th Aero-space Sciences Meeting & Exhibit* (Reno, NV, 2002) AIAA Paper No. 0385, 20 p.
15. C. N. Aliaga, M. S. Aubé, G. S. Baruzzi and W. G. Habashi, Journal of Aircraft **48**(1), 119–126 (2011).
16. J. E. Dillingh and H. W. M. Hoeijmakers, "Accumulation of ice accretion on airfoils during flight", in *Federal Aviation Administration In-flight Icing and Aircraft Ground De-icing Conference* (Chicago, Illinois, 2003) 13 p.
17. J. Hospers and H. W. M. Hoeijmakers, "Numerical Simulation of SLD Ice Accretions", in *Proceedings SAE 2011 (online)* (Chicago, USA, 2011), pp. 1-18.
18. D.Pena, Y. Haorau and E. Laurendeau, Journal of Fluids and Structures **65**, 278–294 (2016).
19. A. AL-Kebsi, D. Pena, E. Laurendeau, R. Mose and Y. Hoarau, "Multi-Step Level-Set Ice Accretion Simulation with the NSMB solver", in *23ème Congrès Français de Mécanique* (Lille, 2017), 14 p.
20. S. Bourgault-Côté, "Simulation du givrage sur ailes en flèche par methods RANS/eulérienne quasi stationnaires", Master thesis, École Polytechnique de Montréal, 2015.
21. S. Bourgault-Côté, S. Ghasemi, A. Mosahebi, and E. Laurendeau, AIAA Journal **55**(2), 662–667 (2017).
22. A. A. Aksenov, Computer Research and Simulation **9**(1), 5-20 (2017). (in Russian)
23. S. V. Zhluktov and A. A. Aksenov, Computer Research and Simulation (in Russian) **7**(6), 1221-1239 (2015).
24. S. V. Zhluktov, A. A. Aksenov and D. V. Savitskiy, Computer Research and Simulation **10**(4), 461–481 (2018). (in Russian)
25. C. Crowe, M. Sommerfeld and Yu. Tsuji, *Multiphase Flows with Droplets and Particles* (CRC Press LLC, 1998), 471 p.
26. B. Abramzon and W. A. Sirignano, Int. J. of Heat and Mass Transfer **32**(9), 1605-1618 (1989).
27. S. V. Alekseenko and A. A. Prihod'ko, Proceedings of TsAGI **XLIV**(6), 25-57 (2013). (in Russian)